

Article

Abrupt Spin Crossover Behavior in a Linear *N1,N2*-Triazole Bridged Trinuclear Fe(II) Complex

Ai-Min Li ^{1,2} , Tim Hochdörffer ³, Juliusz A. Wolny ³, Volker Schünemann ³
and Eva Rentschler ^{1,*} 

¹ Institute of Inorganic and Analytical Chemistry, Johannes Gutenberg University Mainz, Duesbergweg 10-14, 55128 Mainz, Germany; liaimin1@uni-mainz.de

² Graduate School Materials Science in Mainz, Staudingerweg 9, D-55128 Mainz, Germany

³ Fachbereich Physik, Technische Universität Kaiserslautern, Erwin-Schrödinger-Street 46, 67663 Kaiserslautern, Germany; hochdoer@rhrk.uni-kl.de (T.H.); wolny@physik.uni-kl.de (J.A.W.); schuene@physik.uni-kl.de (V.S.)

* Correspondence: rentschler@uni-mainz.de

Received: 28 June 2018; Accepted: 1 August 2018; Published: 7 August 2018



Abstract: The synthesis, structures and magnetic properties of a new trinuclear spin crossover complex $[Fe^{II}_3(\text{pyrtrz})_6(\text{TsO})_6] \cdot 10H_2O \cdot 2CH_3OH$ (**C2**) and its analogue binuclear $[Fe^{II}_2(\text{pyrtrz})_5(\text{SCN})_4] \cdot 7H_2O$ (**C1**), are reported here. These two compounds are synthesized based on the *pyrrolyl* functionalized Schiff base 1,2,4-triazole ligand 4-((1*H*-pyrrol-2-yl)methylene-amino)-4*H*-1,2,4-triazole (pyrtrz), which represent rare discrete multi-nuclear species, with μ_2 -*N1,N2*-triazole bridges linking the Fe^{II} centers. DC magnetic susceptibility measurements revealed an abrupt single-step spin crossover (SCO) behavior for compound **2** on the central Fe^{II} site and single-crystal X-ray diffraction (173 K) showed that this compound crystallizes in the monoclinic space group (*P21/c*), and multiple intramolecular interactions were found responsible for the abrupt transition. Compound **1** is a binuclear complex with thiocyanate as terminal ligands. This compound stays in high spin state over the whole temperature range and displays weak antiferromagnetic exchange coupling.

Keywords: spin crossover; iron(II); trinuclear; binuclear; 1,2,4-triazole; Schiff bases

1. Introduction

SCO as a phenomenon of molecular bistability can mainly be observed in first row transition metal complexes with a d4–d7 electron configuration in octahedral ligand geometry. Most common SCO coordination compounds reported are based on iron(II) with N-donor ligands that provide the appropriate ligand field. Currently, special attention is given to SCO compounds exhibiting pronounced cooperative behavior. Here, the mononuclear system $[Fe(\text{bpp})_2]^{2+}$ (bpp = 2,6-di{pyrazol-1-yl}pyridine) [1–4], as well as the triazole-based mono-/bi-nuclear $[Fe_2(\text{PMAT})_2]^{4+}$ system [5–8], are among the most frequently reported compounds. Recently, we could enlarge the family of binuclear systems showing multiple SCO steps with reports on thiadiazole and oxadiazole complexes for which the cooperativity was studied in detail [9,10]. Similar to these discrete SCO systems, low nuclearity complexes based on the more simple triazole ligand, i.e., binuclear and trinuclear complexes triple-bridged by *N1,N2*-1,2,4-triazole ligands, are currently receiving great interest [11–15]. This family of compounds shows the attempt and endeavor to explore the famous 1D coordination polymers of general formula $[Fe(\text{Rtrz})_3](X)_2$ (Rtrz = 4-substituted-1,2,4-triazole, X^- = standard monoanions): some of which displayed wide thermal hysteresis loops around room temperature [11–16]. Compared to the typical molecular system mentioned above [1–10], the triazole-based compounds bear benefits of expanding the discrete nuclearities to multinuclear or 1D polymeric complexes, which is of vital importance

in the exploration of cooperativity between the covalently linked iron(II) centers. After the first structural report on the 1D polymeric structure $[\text{Fe}(\text{NH}_2\text{trz})_3](\text{NO}_3)_2$ in 2011 [17], there is only one more crystal structure found very recently [18]. However, a series of discrete di-, and tri-nuclear complexes were synthesized and studied, with the intention of better understanding of the 1D polymer at the molecular and inter-molecular scales, such to understand and fine-tune its SCO properties. A detailed summary of these reported discrete *N1,N2*-1,2,4-triazole bridged complexes has been made (Tables S1 and S2), including five excellent results published very recently [19–23]. The diverse while short list of this family of compounds reveals the long-lasting efforts and smooth progress towards uncovering the mystery of the cooperativity of the SCO behavior. Interestingly, among the limited examples of the discrete polynuclear complexes that displayed SCO, the only four trinuclear complexes with *p*-tolylsulfonate (Tos^-) as counteranion [19,24–26] all showed gradual transition with different transition temperatures (Tables S1 and S2). It is suggested that the presence of multiple aromatic anions makes the molecular species well separated, thus a weak communication between the SCO units is presented, which further leads to the gradual spin transition [19,26]. In the present work, we report the first example of a trinuclear complex showing an abrupt spin transition with tolylsulfonate (Tos^-) as counteranion. We report the synthesis, structure, and magnetic properties of two poly-nuclear triazole-bridged Fe^{II} complexes based on a Schiff base modified triazole ligand, i.e., 4-((1*H*-pyrrol-2-yl)methylene-amino)-4*H*-1,2,4-triazole (pyrtrz): $[\text{Fe}^{\text{II}}_2(\text{pyrtrz})_5(\text{SCN})_4]\cdot 7\text{H}_2\text{O}$ (**1**) and $[\text{Fe}^{\text{II}}_3(\text{pyrtrz})_6(\text{TsO})_6]\cdot 10\text{H}_2\text{O}\cdot 2\text{CH}_3\text{OH}$ (**2**). Single X-ray diffraction and magnetic measurement reveal that both compounds are bridged by μ_2 -*N1,N2*-1,2,4-triazole ligands. Compound **1** is a binuclear Fe^{II} complex showing weak antiferromagnetic exchange coupling, while compound **2** is a trinuclear Fe^{II} complex exhibiting an abrupt spin transition behavior. Multiple intramolecular interactions were found being responsible for the sharp transition.

2. Experimental Section

2.1. General Methods and Materials

All commercially purchased chemicals (Alfa Aesar, Karlsruhe, Germany; Sigma-Aldrich, Taufkirchen, Germany; and Acros Organics, Geel, Belgium) and solvents were used without further purification. Magnetic susceptibility data were collected with SQUID magnetometer MPMS XL-7 in a temperature range of 2–300 K with an applied field of 1000 Oe. Samples for SQUID measurement were prepared in gelatin capsules and held in plastic straws for insertion into the magnetometer. The obtained magnetic susceptibility values were corrected for diamagnetic susceptibility according to the Pascal's constants [27]. ^{57}Fe Mössbauer spectra were recorded in transmission geometry using a constant acceleration spectrometer operated in conjunction with a 512-channel analyzer in the time-scale mode (WissEl GmbH, Starnberg, Germany). The source contained ^{57}Co diffused in Rh with an activity of 1.4 GBq. The spectrometer was calibrated against α -iron at room temperature (RT). Variable temperature measurements were performed with a continuous flow cryostat (Optistat^{DN}, Oxford Instruments, Abingdon, UK). Spectral data were transferred from the multi-channel analyzer to a PC for further analysis employing the public domain program Vinda running on an Excel 2003[®] platform [28]. The spectra were analyzed by least-squares fits using Lorentzian line shapes, Γ . Elemental analysis (C, H, and N) was measured in the microanalytical laboratories at Johannes Gutenberg University Mainz. Infrared spectra (FT-IR) were recorded as potassium bromide pellets in the range from 4000 to 400 cm^{-1} with a JASCO FT/IR-4200 at the Johannes Gutenberg-University Mainz.

2.2. Single Crystal X-ray Diffraction

Single-crystal X-ray diffraction data (**C1** and **C2**) were collected on a Bruker Smart APEX II CCD diffractometer. The diffractometer was operated at 45 kV and 35 mA with Mo $K\alpha$ radiation ($\lambda = 0.71073 \text{ \AA}$), and a nitrogen cold stream was applied to keep the collection temperature at 173(2) K. Data reduction was performed using the SAINT and SMART softwares [29] and an empirical

absorption correction was applied with the SADABS program [30]. Both structures (**C1** and **C2**) were solved by direct methods, refined by full-matrix least-squares on F^2 with the SHELXTL program package [31,32], and the Olex2 program [33]. The ordered non-hydrogen atoms in each structure were refined with anisotropic displacement parameters, while the hydrogen atoms were placed in idealized positions and allowed to ride on their parent atoms. In compound **1**, the C39 and S4 atoms are disordered over two positions with a ratio of 2:1, respectively. In compound **2**, the refinement of the reflection data yielded acceptable resolved structural results with highly disordering fragments: there are four disordering positions over the *pyrrolyl* fragments (C31 to C35, N36; N54, C56, N57, C58 to C60; N42, C43 to C47, N48; C67 to C71, N72), all with a ratio of 1:1, and four more disordering positions were found over the counter anion *p*-toluenesulfonate parts (C94 to C100, S4, O16 to O18; C87 to C93; C208 to C214, S6, O22 to O24; C101 to C107, S5, O19 to O20), all with a ratio of 1:1. Even though, with all these disordering positions, we managed to get a final refinement with the final R_1 ($I > 2\sigma(I)$) value of 0.0852 (completeness of 0.996), the major part of the structure is still reliable and gives us valuable data for the structure and property investigation (see in the main text). In all the structures, the lattice water molecules were refined with anisotropic displacement parameters, while the hydrogen atoms were not defined. Thus, in the discussion of the main text, unless specified, all the lattice water molecules or the disordered parts were not included. The crystallographic data and refinement parameters of **C1** and **C2** are listed in Table 1. CCDC numbers 1,815,489–1,815,490 contain the supplementary crystal data of the compounds: 1,815,489 (**C1**) and 1,815,490 (**C2**), which can be obtained free of charge from The Cambridge Crystallographic Data Centre via www.ccdc.cam.ac.uk/data_request/cif. All structure figures are generated with DIAMOND-3 [34].

2.3. Syntheses

2.3.1. Synthesis of the Ligand

The ligand 4-((1*H*-pyrrol-2-yl)methylene-amino)-4*H*-1,2,4-triazole (pytrtz) (Figure 1) was prepared by the condensation reaction [35,36]: 4-Amino-1,2,4-triazole (1.68 g, 0.02 mol, 1.0 eq.) and pyrrole-2-carboxaldehyde (2.09 g, 0.022 mol, 1.1 eq.) were dissolved in ethanol with the addition of few drops of H_2SO_4 , acting as acidic catalyst. The reaction mixture was slowly heated up to 80 °C until it started to boil, then kept refluxing for 10 h. When it cooled down to r.t., the excess of the solvent was removed by rotary evaporator at 35 °C. The products such obtained was washed with small amount of cold ethanol, diethyl ether and then dried in the desiccator with phosphorus pentoxide as dry agent. Dark purple powder was obtained. Yield: 3.14 g (97.5%), m.p., 207.5–210.7 °C; IR (KBr): 1635 cm^{-1} (vw), 3127 (w), 1169 (s), 1062 (vs), 860 (s), 762 and 621 cm^{-1} (Ar, CH-strech); 817 cm^{-1} , 2918 cm^{-1} (Ar-CH₃). ¹H-NMR (Figure S1) (CD₃OD) 7.91 (s, 1H, Ar-H), 7.99 (s, 1H, Ar-H), 8.92 (s, 1H, H-C=N), 9.07 (s, 2H, triazole).

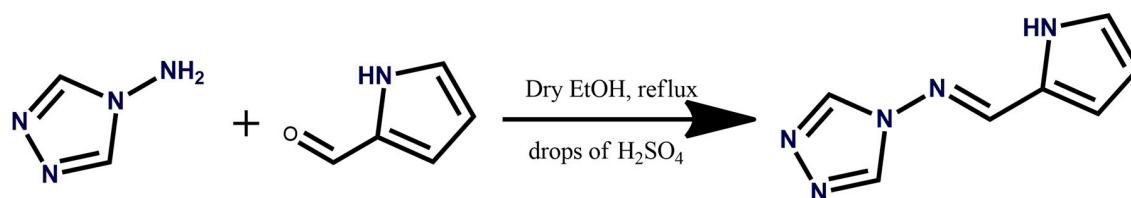


Figure 1. Synthetic scheme to prepare the pytrtz ligand.

2.3.2. Synthesis of the Complex

Synthesis of $[Fe^{II}_2(pytrtz)_5(SCN)_4] \cdot 7H_2O$ (**C1**)

To a stirring solution of pytrtz (129 mg, 0.8 mmol) in methanol (5 mL) was added an aqueous solution of $FeSO_4 \cdot 7H_2O$ (90 mg, ≈ 0.3 mmol) and NH_4SCN (50 mg, ≈ 0.6 mmol). The solution turned

from light purple to dark red immediately. To prevent possible oxidation process, one spatula amount (≈ 35 mg) of ascorbic acid was added into the reaction solution. The reaction mixture was then stirred for around 3–4 h before filtrated with rapid filter paper. The clear light reddish solution such obtained was kept in a small vial and left stand still to allow the solvent evaporate slowly. After one week, light brown block-like crystals of **C1** were deposited at the bottom of the vial. After removing the mother liquid, the single crystals were quickly dried in an argon stream, and stored under argon. Yield: 127.1 mg (34.9% based on Fe). Anal. Calcd (Found) for $C_{39}H_{49}Fe_2N_{29}O_7S_4$: C, 36.71 (36.38); H, 3.87 (3.63); N, 31.83 (32.62). IR (KBr) n/cm^{-1} : 3125 (w), 2927 (m), 2856 (w), 2078 (s), 1609 (vs), 1523 (m), 1422 (w), 1385 (vs), 1311 (m), 1246 (vs), 1127 (s), 1063 (m), 1037 (m), 985 (m), 881 (w), 759 (m), 621 (s), 593 (m), 506 (w).

Synthesis of $[Fe^{II}_3(\text{pyrtrz})_6(\text{TsO})_6] \cdot 10H_2O \cdot 2CH_3OH$ (**C2**)

Freshly prepared $Fe(\text{TsO})_2$ (120 mg, ≈ 0.3 mmol) in 3 mL H_2O was added into a stirring solution of pyrtrz (97 mg, 0.6 mmol) dissolved in MeOH (2–3 mL). After stirring for half hour, one spatula amount (≈ 35 mg) of ascorbic acid was added. This solution was then stirred for 3–4 h before filtrated. The obtained clear light yellow solution was then kept in a small vial and left stand still to evaporate the solvent slowly. After two weeks, light pink needle-like crystals of **C2** were deposited at the bottom of the vial. After removing the mother liquid, the single crystals were quickly dried in an argon stream, and stored under argon. Yield: 257.3 mg (35.8% based on Fe). Anal. Calcd (Found) for $C_{86}H_{116}Fe_3N_{30}O_{32}S_6$: C, 42.30 (42.26); H, 4.79 (4.22); N, 17.21 (17.62). IR (KBr) n/cm^{-1} : 3097 (w), 2988 (w), 2922 (w), 2857 (w), 1605 (vs), 1530 (s), 1446 (m), 1423 (m), 1368 (s), 1189 (vs), 1125 (s), 1072 (s), 1035 (vs), 1010 (s), 883 (m), 844 (m), 815 (m), 752 (m), 682 (s), 624 (m), 606 (w), 566 (s), 513 (w).

3. Result and Discussion

3.1. X-ray Crystal Structure Description

Crystallographic data for the compounds **1** and **2** are summarized in Table 1 and the selected bond lengths and angles are presented in Table S3.

Table 1. Crystallographic Data and Refinement Parameters for Compounds **1** and **2**.

Compound	1	2
Empirical formula	$C_{39}H_{49}Fe_2N_{29}O_7S_4$	$C_{86}H_{116}Fe_3N_{30}O_{32}S_6$
Formula weight	1213.90	2393.76
Crystal size	$0.14 \times 0.13 \times 0.07$	$0.51 \times 0.11 \times 0.03$
Crystal system	Triclinic	Triclinic
Space group	$P-1$ (No. 2)	$P121/c1$ (No. 14)
a (Å)	11.9168(13)	19.3399(19)
b (Å)	13.8948(15)	15.6171(15)
c (Å)	18.830(2)	37.287(4)
α (°)	90.543(3)	90
β (°)	101.891(3)	96.902(2)
γ (°)	102.381(3)	90
V (Å ³)	2975.4(6)	1,1180.2(19)
Z	2	4
D_{calc} (g/cm ³)	1.355	1.422
μ (Mo-K α) (mm ⁻¹)	0.691	0.583
$F(000)$	1240	4936
Reflections collected	28,747	64,247
Independent reflections	10,485 (0.1442)	26,617 (0.1035)
Parameters	668	1858
Goodness-of-fit	0.919	0.996
R_1 [$I > 2\sigma(I)$] ^a	0.1123	0.0852
wR_2 (all data) ^b	0.3641	0.2743

^a $R_1 = \sum ||F_o| - |F_c|| / \sum |F_o|$, ^b $wR_2 = \{\sum [w(F_o^2 - F_c^2)^2] / \sum [w(F_o^2)^2]\}^{1/2}$.

3.1.1. Crystal Structure of $[\text{Fe}^{\text{II}}_2(\text{pyrtrz})_5(\text{SCN})_4] \cdot 7\text{H}_2\text{O}$ (C1)

Compound **1** crystallizes in the triclinic space group $P-1$. The asymmetric unit contains one full neutral binuclear complex plus 7 lattice water molecule positions. However, some of these positions are partially occupied resulting in a total of 4 water molecules in the structure. As shown in Figure 2, for each molecule, the two Fe^{II} centers are linked through three μ_2 - $N1,N2$ -triazole bridges with the distance of 3.988(7) Å. Each Fe^{II} coordination sphere is further completed by one nitrogen (N16 and N22) atom from the terminal triazole ligand, two nitrogen (N26, N27 and N28, N29) atoms via *cis*-thiocyanate anions. The terminal average Fe–N bond length of 2.113(3) Å is shorter than the central average Fe–N bond length of 2.159(3) Å (Table S3). In both cases, the bond distance confirms the Fe centers being in the high-spin state at 173 K [37], which is further confirmed by magnetic measurements (see below). The NCS^- anions are almost linear with the N–C–S angle around 178°; the angle of coordination to iron Fe–N–C is split into two groups with the angle being around 160° and 175° (Table S3). Within the structure, one of the terminal thiocyanates is disordered over the $\text{C}_{39}\text{--S}_4$ bond part with a relative occupancy of 2:1.

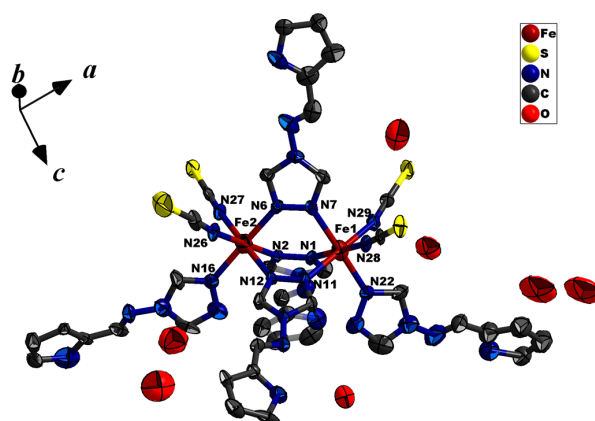


Figure 2. Thermal ellipsoid view of the binuclear molecular structure of **C1** at 173 K, shown with 40% probability ellipsoids. All H atoms are omitted, and only selected atoms are labelled for clarity.

In compound **1**, the adjacent neutral binuclear units are interconnected through $\text{C}_{31}\text{--H}_{31} \cdots \pi_{\text{N15-ring}}$ stacking ($\text{C}_{31}\text{--H}_{31} \cdots \text{centroid} = 2.6070(2)$ Å) and a group of one-to-two H-bonding ($\text{S}_4 \cdots \text{H}_{17} = 2.9763(3)$ Å, $\text{S}_4 \cdots \text{H}_{16} = 2.6145(2)$ Å) interactions to form a 1D chain along a axis. (Figure 3) This chain is further connected in bc plane through another two groups of parallel intermolecular $\pi \cdots \pi$ stacking (centroid \cdots centroid 3.5625(2) Å) together with one set of $\text{C}_6\text{--H}_6 \cdots \pi_{\text{N5 ring}}$ stacking ($\text{C}_6\text{--H}_6 \cdots \text{centroid} = 3.7232(5)$ Å) to form a 3D supramolecular architecture (Figure 4).

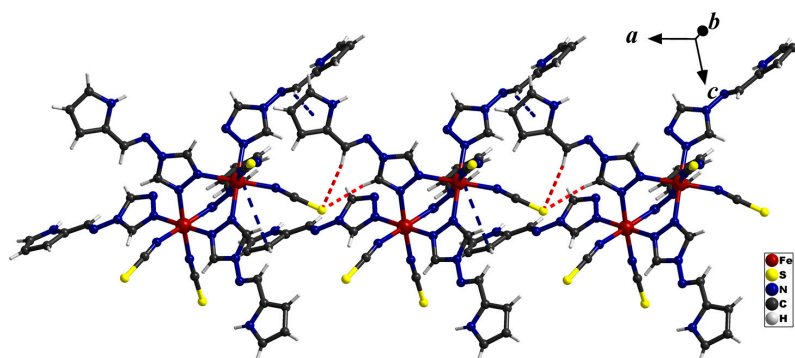


Figure 3. The 1D chain connected via different intermolecular interactions along a axis. The red dashed lines represent H-bonding, while the blue dashed lines represent $\pi \cdots \pi$ stacking.

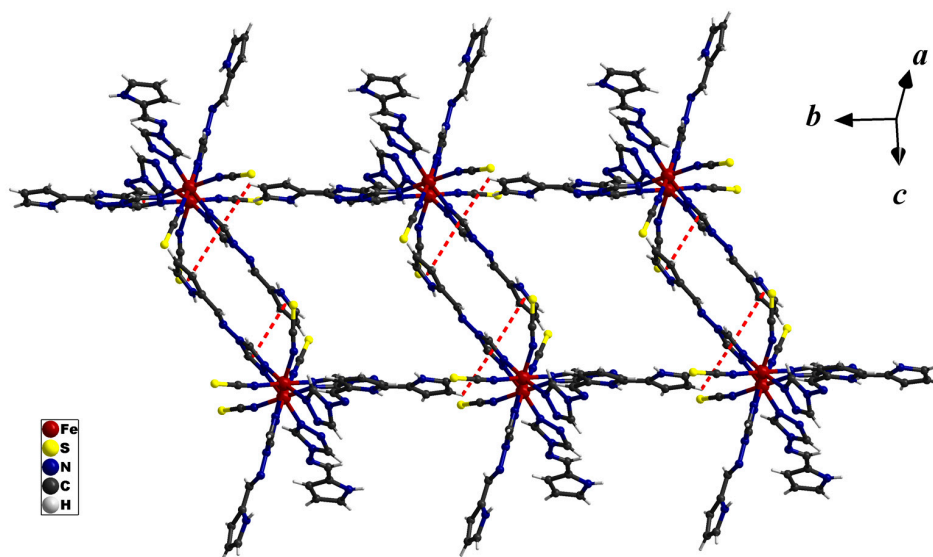


Figure 4. The $\pi \cdots \pi$ stacking in bc plane of compound 1.

3.1.2. Crystal Structure of $[\text{Fe}^{\text{II}}_3(\text{pyrtrz})_6(\text{TsO})_6] \cdot 10\text{H}_2\text{O} \cdot 2\text{CH}_3\text{OH}$ (C2)

Compound 2 crystallizes in monoclinic space group $P21/c$. Within the linear trinuclear basic units, the Fe^{II} ions are linked by three μ_2 - $N1, N2$ -donating triazole ligands, the terminal coordination sites are occupied by three H_2O molecules to complete the $[\text{N}_3\text{O}_3]$ hexa-coordination (Figure 5). Quite surprisingly, this structure consists of three complete Fe centers within the asymmetrical units, where there are only three other examples among the 17 reported linear trimer analogues, including one new example published February this year (2018) (Table S2) [21,22,38]. While the central Fe2 is in an octahedral $[\text{FeN}_6]$ coordination environment, the outer Fe^{II} ion, Fe1 and Fe3, are in a $[\text{FeN}_3\text{O}_3]$ coordination environment due to the coordination of the terminal water molecules. Each trinuclear unit is cationic with a 6+ charge, which is balanced by six free *p*-toluenesulfonate counteranions. Interestingly, due to different groups of H-bonding and π stacking (Figure 6, Tables S4 and S5), the *p*-toluenesulfonate ions are distributed unequally around the three linear Fe units. This unique feature makes the Fe centers crystallographically independent reflected by the monoclinic space group with three independent Fe centers within the asymmetrical unit. The X-ray analysis also reveals two methanol and ten water molecules linked to the trinuclear units via different H-bonding interactions, as some atoms are only partially occupied, resulting only in a total of one methanol and 6.5 water molecules identified. The hydrogen atoms from the water molecules are not defined here, thus potential supramolecular interactions involved are not discussed here. Though a significant point needed to be pointed out is that six out of the ten water molecules scattered exclusively along one side of the trimer with another one (O29) embedded in the middle of the trimer units. The uneven distribution of the water molecules is balanced by the unequally distributed *p*-toluenesulfonate anions. This further supports the uniqueness of the structure (Figure 5).

According to the ligand field theory, the total ligand-field strength is larger for the central iron center (coordinated by six triazole N atoms) than for the peripheral ions (surrounded by three triazole N and three O atoms from water). Considering the coordination environment among the three crystallographically unique iron(II) ions, only the central one (Fe2) is in the expected coordination environment for SCO to occur. According to the magnetic susceptibility measurement, the spin transition between the central Fe^{II} sites occurs between 150–95 K with $T_{1/2}$ around 120 K (details see the magnetic part). The crystal structure determination was conducted at 173 K, right in the beginning of the spin transition. While still, significant differences were observed between the central Fe and the peripheral ones. The examination of the Fe2–N distances reveals bond lengths of approximately 2.08 Å (Table S3) which are consistent with this site being in between the LS and HS state at this

temperature. The Fe1–N and Fe3–N bond distances of approximately 2.16 Å are consistent with a HS state as expected for this coordination environment (Table S3, Figure 7).

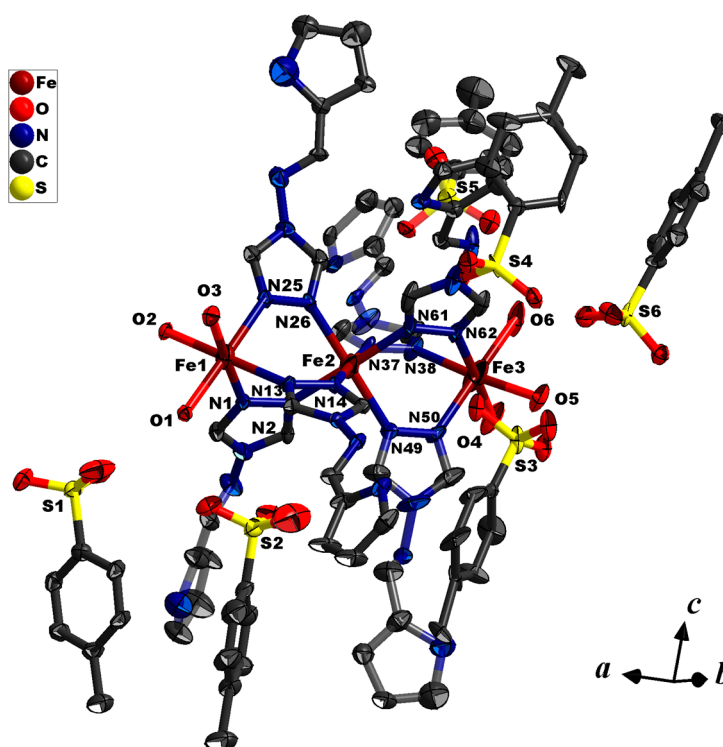


Figure 5. Thermal ellipsoid view of the linear trinuclear complex C2 at 173 K, shown with 40% probability ellipsoids. All water, methanol solvent molecules and H atoms are omitted for clarity, and only selected atoms are labelled.

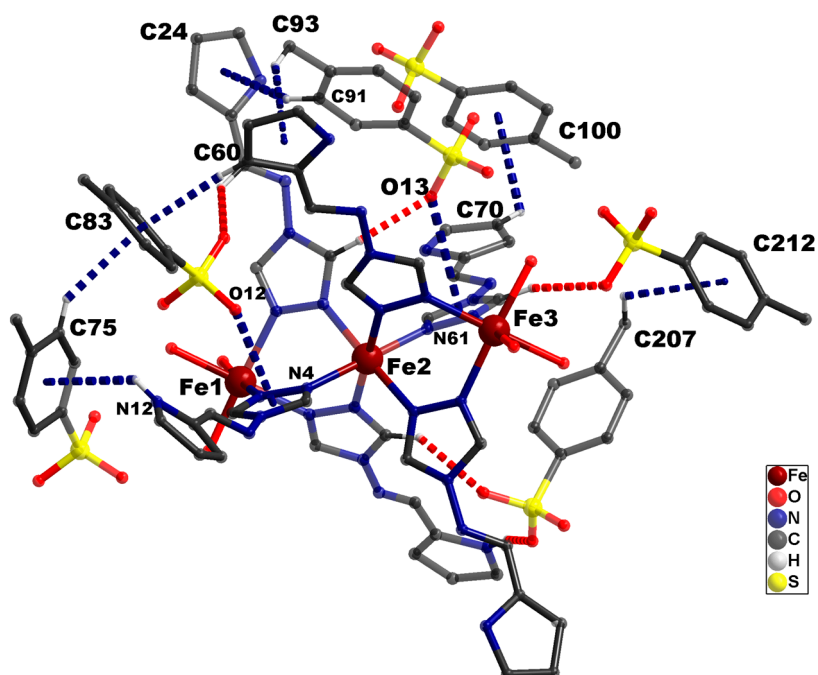


Figure 6. The different intramolecular interaction found in the trimer units. The red dashed lines represent H-bonding, while the blue dashed lines represent π - π stacking.

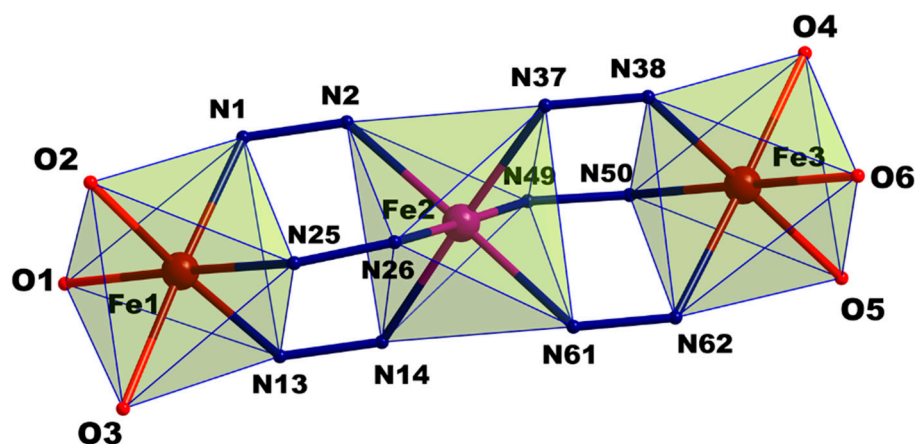


Figure 7. Labeled core of the linear trinuclear complex. Iron(II) sites (spheres) are coloured differently to distinguish the spin state (high spin (HS): red, low spin (LS): purple).

Numerous intra- and inter-molecular interactions involving the sulfonate oxygen atoms of the free *p*-tolylsulfonate anions lead to the final crystal packing. These supramolecular interactions explain the unusual sharp transition found in the rather bulky π -rich (conjugated) ligand system [19,26]. A comprehensive list of all the interactions is given in Table S5.

3.2. FT-IR Spectroscopy

The FT-IR spectra of compounds **1** and **2** indicate that the coordinated ligand pytrz here almost exhibits the same vibrations to that in the neat form pytrz. As shown in Figure 8, the spectra of the two compounds are very similar and are dominated by the spectral characteristics of the Schiff base ligand. However, a careful inspection allows the assignment of significant changes due to the coordination in the complexes. The vibration frequencies of the aromatic groups ($C_{ar}-C_{ar}$ and $C_{ar}=N$) can be found between 1310 cm^{-1} and 1610 cm^{-1} in both compounds and the free ligand. The peak at 1508 (s, pytrz), 1522 (m, **C1**) and 1529 (s, **C2**) cm^{-1} can be assigned to the characteristic ω -triazole ring vibration. The $\approx 15\text{ cm}^{-1}$ hypsochromic shifts between the compounds and the free ligand indicate the coordination of nitrogen atoms to the metal centers [39]. Additionally, the peaks at 1169 (s), 1062 (vs), and 762 (vs) cm^{-1} can be assigned to the C–H in-plane or out-of-plane bend ring breathing, and ring deformation absorptions. The characteristic azomethine (HC=N) stretching [40] around 1635 cm^{-1} in the ligand somehow showed as a very faint peak [41]. The spectrum of **C2** showed strong C=N stretching at 2078 cm^{-1} suggesting the presence of the thiocyanate in the compounds. The 28 cm^{-1} hypsochromic shift compared to the spectrum of KNCS (2050 cm^{-1}) indicates the fact that SCN is coordinated to Fe^{II} via the nitrogen atoms [42,43]. In addition, the spectrum of **C1** showed signature bands for the *p*-toluenesulfonate counterions: The band at 1446 cm^{-1} could be ascribed to the $-\text{CH}_3$ vibrations of the anion, and the bands at 1035 , 1010 cm^{-1} may be assigned to the internal vibrations of the $\text{CH}_3\text{C}_6\text{H}_4$ parts [44]. While the broad band at 1189 cm^{-1} and sharp one at 1125 cm^{-1} are assigned to $\nu_{as}(-\text{SO}_3^-)$ and $\nu_{s}(-\text{SO}_3^-)$ vibrations, respectively.

3.3. Magnetic Susceptibility and Mössbauer Spectroscopy

As shown in Figure 9, the magnetic susceptibility data of compound **1** has been recorded in the temperature range $300\text{--}2\text{ K}$. The $\chi_{\text{M}}T$ value of $6.55\text{ cm}^3\cdot\text{K}\cdot\text{mol}^{-1}$ (**C1**) at 300 K can be ascribed to the corresponding two high spin Fe(II) ions. This value remains almost constant at $6.55\text{--}6.27\text{ cm}^3\cdot\text{K}\cdot\text{mol}^{-1}$ for compound **1** from 300 K down to 140 K ; below this temperature, it starts to decrease more and more abruptly to reach a final value of $0.88\text{ cm}^3\cdot\text{K}\cdot\text{mol}^{-1}$ (2 K). This temperature dependent behavior indicates typical antiferromagnetic magnetic coupling between the two Fe(II) ions in the high spin state.

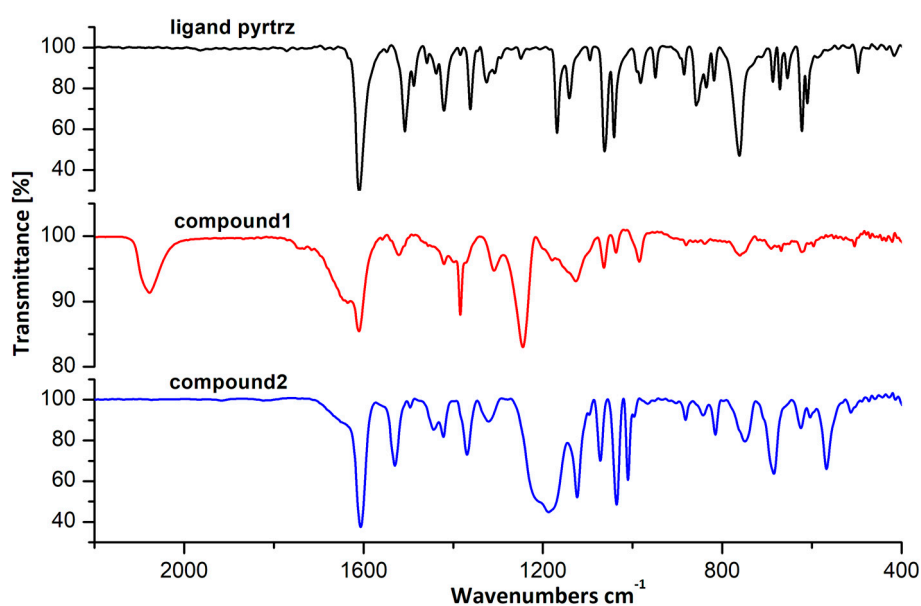


Figure 8. The FT-IR spectra of ligand pytrtz and compounds 1, 2.

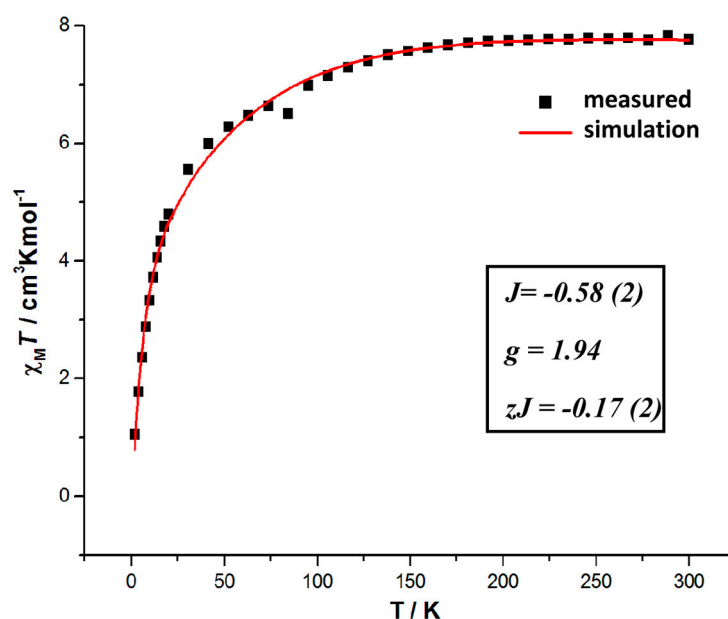


Figure 9. The temperature-dependent magnetic susceptibility for compound 1 (the solid line represents the best fit curve).

To evaluate the antiferromagnetic coupling through the triple *N1,N2*-triazole bridge in the binuclear complex, the magnetic data are simulated with the PHI [45] program over the entire temperature range. Considering the multiple supramolecular interactions found between the adjacent dimer molecules, the intermolecular interaction parameter zJ was implemented with the fitting progress. The best fitting result gives us the values $g = 1.94$, $zJ = -0.17(2) \text{ cm}^{-1}$ with coupling constant $J = -0.58(2) \text{ cm}^{-1}$ (Figure 9). The result suggests that the antiferromagnetic coupling between the two adjacent Fe(II) centers is weak, and the supramolecular interactions found in the crystal lattice was found assisting for the antiferromagnetic coupling.

Temperature dependent magnetic susceptibility measurements on a bulk crystalline sample of compound 2 was also made from 300 K to 4 K range. As illustrated in Figure 10, the magnetic

susceptibility data reveal an abrupt one-step SCO. At 300 K, the $\chi_M T$ values of $9.63 \text{ cm K mol}^{-1}$ are in agreement with all Fe(II) sites being in the HS state per trinuclear unit. This value remains approximately constant until 150 K where the decrease in $\chi_M T$ values becomes abruptly all the way down to $6.75 \text{ cm} \cdot \text{K mol}^{-1}$ at 95 K. This process indicates a sharp SCO transition of one-third of the Fe(II) sites to the LS state with a $T_{1/2}$ around 120 K. No thermal hysteresis was observed.

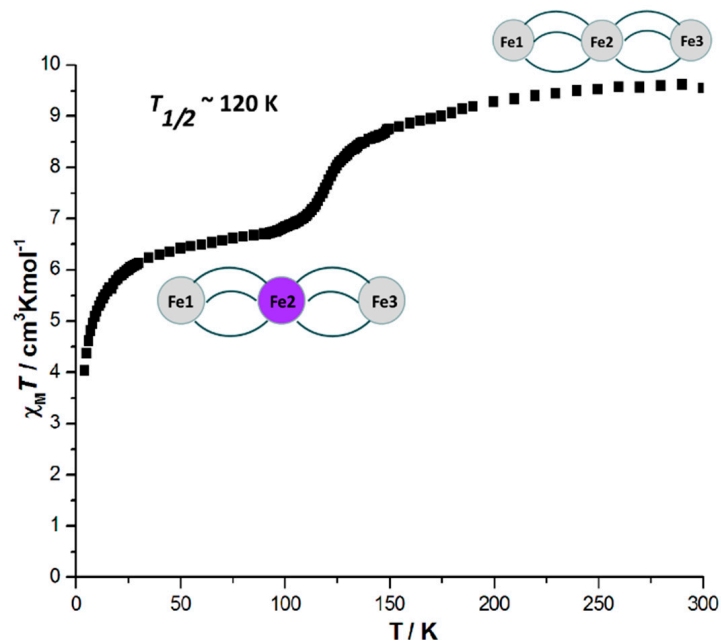


Figure 10. The temperature-dependent magnetic susceptibility ($\chi_M T$ vs. T) for compound 2.

In order to understand the details of SCO process of compound 2, temperature dependent Mössbauer spectroscopy was performed on a bulk crystalline sample (Figure 11). Spectra were recorded at 77 K, 107 K, 137 K, 167 K and 197 K. The spectra have been analyzed with in total 3 different subspectra. The full parameters (δ : isomer shift, ΔE_Q : quadrupole splitting, Γ : line width at half maximum, A : relative spectral area) are listed in Table 2.

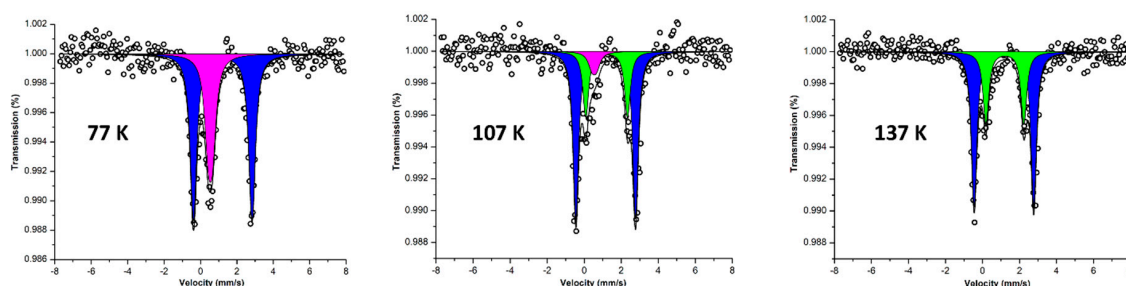


Figure 11. Mössbauer spectra of compound 2 at 77 K, 107 K and 137 K. The open circles are the experimental data, the black solid line shows a superposition of the following components: subspectrum 1 (purple) represents the [LS] fraction of central iron (Fe2), subspectrum 2 (blue) is due to the [HS] fraction of terminal iron (Fe1 and Fe3), and subspectrum 3 (green) is the [HS] fraction of central iron (Fe2). Parameters see Table 2.

Table 2. ^{57}Fe Mössbauer parameters of compound **2** at different temperatures.

T = 77 K			
Subspectra	HS Fe1 and Fe3	LS Fe2	HS Fe2 and Fe3
δ [mm/s]	1.22 ± 0.02	0.54 ± 0.04	-
ΔE_0 [mm/s]	3.22 ± 0.02	0.24 ± 0.03	-
Γ [mm/s]	0.41 ± 0.03	0.47 ± 0.03	-
Rel. Area [%]	66.00 ± 1.00	34.00 ± 1.00	0
T = 107 K			
δ [mm/s]	1.16 ± 0.03	0.54 ± 0.05	1.21 ± 0.04
ΔE_0 [mm/s]	3.22 ± 0.04	0.24 ± 0.10	2.25 ± 0.02
Γ [mm/s]	0.34 ± 0.02	0.47 ± 0.07	0.36 ± 0.04
Rel. Area [%]	65.00 ± 1.00	8.00 ± 2.00	27.00 ± 1.00
T = 137 K			
δ [mm/s]	1.16 ± 0.03	-	1.21 ± 0.03
ΔE_0 [mm/s]	3.22 ± 0.04	-	2.05 ± 0.04
Γ [mm/s]	0.34 ± 0.02	-	0.44 ± 0.03
Rel. Area [%]	65.00 ± 2.00	-	35.00 ± 1.00
T = 167 K			
δ [mm/s]	1.15 ± 0.02	-	1.21 ± 0.04
ΔE_0 [mm/s]	3.16 ± 0.02	-	1.93 ± 0.03
Γ [mm/s]	0.34 ± 0.01	-	0.36 ± 0.05
Rel. Area [%]	64.00 ± 2.00	-	36.00 ± 2.00
T = 197 K			
δ [mm/s]	1.15 ± 0.04	-	1.21 ± 0.03
ΔE_0 [mm/s]	3.16 ± 0.04	-	1.87 ± 0.04
Γ [mm/s]	0.34 ± 0.02	-	0.36 ± 0.01
Rel. Area [%]	67.00 ± 1.00	-	33.00 ± 1.00

As clearly shown in Figure 11 and Table 2, the Mössbauer spectrum at 77 K shows two distinctly different doublets. Doublet 1 (purple) has $\delta = 0.54 \text{ mm}\cdot\text{s}^{-1}$ and $\Delta E_Q = 0.24 \text{ mm}\cdot\text{s}^{-1}$. Such a low quadrupole splitting is characteristic for a LS iron(II) embedded in an octahedral ligand field. Doublet 2 (blue) has $\delta = 1.22 \text{ mm}\cdot\text{s}^{-1}$ and $\Delta E_Q = 3.22 \text{ mm}\cdot\text{s}^{-1}$, values which are typical fingerprints of a high-spin iron(II) species in an octahedral N/O ligand environment [46]. The relative intensity ratio of 1:2 between these two doublets indicates that the central iron(II) is in its low spin state, i.e., for complex **2**, a HS-LS-HS state is stabilized at 77 K, which is in accordance with the magnetic susceptibility results discussed above. With increasing temperature, at 107 K, the intensity of doublet 1 representing the central LS iron(II) decreases while a new doublet 3 (green) emerges which has $\delta > 1 \text{ mm}\cdot\text{s}^{-1}$, an isomer shift typical for Fe(II) HS. The SCO of the central Fe is perfectly reflected in the Mössbauer spectra displayed at this temperature (at 107 K), that is, the intensity increasing of the green doublet 3 (central iron HS) is at the expense of the decreasing intensity of the purple doublet 1 (central iron LS). It is worth noticing that the intensity of LS and HS species here does not reflect the actual concentrations of the different iron sites because of the different Lamb-Mössbauer factors for the LS and HS state [25,47,48]. Nevertheless, the total intensity sum of green doublet 3 and purple doublet 1 still keeps a 1:2 ratio to the blue doublet 2 (external iron HS), confirming the SCO process undergoing on the central iron center only. At 137 K, doublet 1 vanishes, and the approximate 2:1 relative area ratio of the HS doublet 2 and the HS doublet 3 reflects the SCO transition of complex **2** from a HS-LS-HS state to a HS-HS-HS state. Further measurements of higher temperature (167 K and 197 K) reveal good agreement with the steady HS and LS ratio of 1:2, which confirms the stability of HS-HS-HS state after the spin transition. Additionally, the relative intensity ratio of 3:1 between the green doublet 3 and purple doublet 1 at 107 K gives us the hint of the transition temperature being around 120 K. As the

spin transition in compound **2** is abrupt, with the help of the derivative plot of the $\chi_M T$ vs. T curve (Figure S2), a spin transition temperature of 120 K is also easily spotted. In conclusion, the temperature dependent Mössbauer spectra displayed in Figure 11 clearly shows that the central iron(II) in complex **2** is able to undergo SCO with $T_{1/2}$ around 120 K, which is in good accordance with the magnetic susceptibility data shown in Figure 10.

The abrupt SCO behavior of this compound suggests medium strong cooperativity between molecules in the lattice, which is in accordance with the structural analysis. The multiple intra- and inter-molecular H-bonding interactions found in the crystal lattice explain the strong cooperativity between the active Fe(II) centers. Interestingly, even though studies have shown that ligands with bulky aromatic substituents and aromatic anions might have a “dilute or separation effect” on the overall cooperativity of the SCO compounds [19,26]. The abrupt transition observed here stands for an example with the supramolecular interactions overcome the “aromatic dilute effect”. A further study can be followed by synthesis of similar compounds with different degree of aromatic substitutions, either from the triazole ligands or from the counter anions. Furthermore, the relatively low transition temperature (120 K) for this compound is consistent with other similar discrete molecular species containing bulky aromatic 1,2,4-triazole ligands [19,24–26].

4. Conclusions

The work presented here shows two new examples of discrete triazole-based multi-nuclear Fe^{II} complexes. Based on the ligand 4-((1H-pyrrol-2-yl)methylene-amino)-4H-1,2,4-triazole (pyrtrz), a group of two crystalline coordination Fe^{II} complexes, i.e., one binuclear $[Fe^{II}_2(pyrtrz)_5(SCN)_4] \cdot 7H_2O$ (**C1**) and one trinuclear $[Fe^{II}_3(pyrtrz)_6(TsO)_6] \cdot 10H_2O \cdot 2CH_3OH$ (**C2**), has been synthesized and magnetically characterized. An abrupt spin transition ($T_{1/2} = 120$ K) was found in compound **2**, which was confirmed and explored by the magnetic susceptibility, Mössbauer spectra and structural measurements. The binuclear complex **1** did not show the spin transition, while a weak antiferromagnetic exchange coupling inside the dimer molecules was detected, assisted by the supramolecular interactions in the crystal lattice. The trimer complex described here represent the first example of an abrupt transition found with the accompanying of tolylsulfonate anion. This work suggests that apart from the inefficient communication the bulky aromatic groups might bring into the SCO system, the multiple supramolecular interaction formed can sometimes also lead to a good cooperativity between the active metal centers. The future work might need to focus on the isolation of more similar compounds with different degree of potential supramolecular interactions to examine their effect more quantitatively.

Supplementary Materials: The following are available online at <http://www.mdpi.com/2312-7481/4/3/34/s1>.

Author Contributions: A.-M.L. and E.R. conceived and designed the experiments. Synthesis and characterization, including X-ray diffraction data refinement and magnetic measurements were carried out by A.-M.L. Mössbauer data measurements and analysis were carried out by T.H., J.A.W. and V.S. The manuscript was prepared and edited by A.-M.L. and E.R.

Acknowledgments: We kindly thank Dieter Schollmeyer and Regine Jung-Pothmann (Johannes Gutenberg University, Mainz) for collecting the crystal structural data. A.M.L. acknowledges the financial support from graduate school MAINZ and is a recipient of a DFG fellowship through the Excellence Initiative by the Graduate School Materials Science in Mainz (DFG/GSC 266). E.R. and V.S. also acknowledge the support of the German Research Foundation (DFG) through the Transregional Collaborative Research Center SFB/TRR173 Spin + X, Projects A04 and A09.

Conflicts of Interest: The authors declare no conflict of interest.

References

1. Halcrow, M.A. Iron(II) complexes of 2,6-di(pyrazol-1-yl)pyridines—A versatile system for spin-crossover research. *Coord. Chem. Rev.* **2009**, *253*, 2493–2514. [[CrossRef](#)]

2. Berdiell, I.C.; Kulmaczewski, R.; Halcrow, M.A. Iron(II) Complexes of 2,4-Dipyrazolyl-1,3,5-triazine Derivatives—The Influence of Ligand Geometry on Metal Ion Spin State. *Inorg. Chem.* **2017**, *56*, 8817–8828. [[CrossRef](#)] [[PubMed](#)]
3. Deeth, R.J.; Halcrow, M.A.; Kershaw Cook, L.J.; Raithby, P.R. Ab Initio Ligand Field Molecular Mechanics and the Nature of Metal-Ligand π -Bonding in Fe(II) 2,6-di(pyrazol-1-yl)pyridine Spin Crossover Complexes. *Chem. Eur. J.* **2018**, *24*, 5204–5212. [[CrossRef](#)] [[PubMed](#)]
4. Kershaw Cook, L.J.; Thorp-Greenwood, F.L.; Comyn, T.P.; Cespedes, O.; Chastanet, G.; Halcrow, M.A. Unexpected Spin-Crossover and a Low-Pressure Phase Change in an Iron(II)/Dipyrazolylpyridine Complex Exhibiting a High-Spin Jahn–Teller Distortion. *Inorg. Chem.* **2015**, *54*, 6319–6330. [[CrossRef](#)] [[PubMed](#)]
5. Feltham, H.L.; Barltrop, A.S.; Brooker, S. Spin crossover in iron(II) complexes of 3,4,5-tri-substituted-1,2,4-triazole (Rdpt), 3,5-di-substituted-1,2,4-triazolate (dpt[−]), and related ligands. *Coord. Chem. Rev.* **2017**, *344*, 26–53. [[CrossRef](#)]
6. Feltham, H.L.; Dankhoff, K.; Meledandri, C.J.; Brooker, S. Towards Dual-Functionality Spin-Crossover Complexes. *Chem. Plus Chem.* **2018**, *83*, 582–589. [[CrossRef](#)]
7. Feltham, H.L.; Cowan, M.G.; Kitchen, J.A.; Jameson, G.N.; Brooker, S. Targeted structural modification of spin crossover complexes: Pyridine vs. pyrazine. *Supramol. Chem.* **2018**, *30*, 296–304. [[CrossRef](#)]
8. Rodríguez-Jiménez, S.; Barltrop, A.S.; White, N.G.; Feltham, H.L.; Brooker, S. Solvent Polarity Predictably Tunes Spin Crossover T_{1/2} in Isomeric Iron(II) Pyrimidine Triazoles. *Inorg. Chem.* **2018**, *57*, 6266–6282. [[CrossRef](#)] [[PubMed](#)]
9. Herold, C.F.; Carrella, L.M.; Rentschler, E. A Family of Dinuclear Iron(II) SCO Compounds Based on a 1,3,4-Thiadiazole Bridging Ligand. *Eur. J. Inorg. Chem.* **2015**, *22*, 3632–3636. [[CrossRef](#)]
10. Köhler, C.; Rentschler, E. The First 1,3,4-Oxadiazole Based Dinuclear Iron(II) Complexes Showing Spin Crossover Behavior with Hysteresis. *Eur. J. Inorg. Chem.* **2016**, *13*, 1955–1960. [[CrossRef](#)]
11. Haasnoot, J.G. Mononuclear, oligonuclear and polynuclear metal coordination compounds with 1,2,4-triazole derivatives as ligands. *Coord. Chem. Rev.* **2000**, *200*, 131–185. [[CrossRef](#)]
12. Aromí, G.; Barrios, L.A.; Roubeau, O.; Gamez, P. Triazoles and tetrazoles: Prime ligands to generate remarkable coordination materials. *Coord. Chem. Rev.* **2011**, *255*, 485–546. [[CrossRef](#)]
13. Roubeau, O. Triazole-based one-dimensional spin-crossover coordination polymers. *Chem. Eur. J.* **2012**, *18*, 15230–15244. [[CrossRef](#)] [[PubMed](#)]
14. Lavrenova, L.G.; Shakirova, O.G. Spin Crossover and Thermochromism of Iron(II) Coordination Compounds with 1, 2, 4-Triazoles and Tris (pyrazol-1-yl) methanes. *Eur. J. Inorg. Chem.* **2013**, 670–682. [[CrossRef](#)]
15. Garcia, Y.; Niel, V.; Muñoz, M.C.; Real, J.A. Spin Crossover in 1D, 2D and 3D Polymeric Fe(II) Networks. In *Spin Crossover in Transition Metal Compounds I*; Gülich, P., Goodwin, H.A., Eds.; Springer: Berlin/Heidelberg, Germany, 2004; Volume 233, pp. 229–257.
16. Kahn, O.; Jay, M.C. Spin-transition polymers: from molecular materials toward memory devices. *Science* **1998**, *279*, 44–48. [[CrossRef](#)]
17. Grosjean, A.; Daro, N.; Kauffmann, B.; Kaiba, A.; Létard, J.F.; Guionneau, P. The 1-D polymeric structure of the [Fe(NH₂trz)₃](NO₃)₂·nH₂O (with n = 2) spin crossover compound proven by single crystal investigations. *Chem. Commun.* **2011**, *47*, 12382–12384. [[CrossRef](#)] [[PubMed](#)]
18. Pittala, N.; Thétiot, F.; Triki, S.; Boukheddaden, K.; Chastanet, G.; Marchivie, M. Cooperative 1D Triazole-Based Spin Crossover FeII Material with Exceptional Mechanical Resilience. *Chem. Mater.* **2016**, *29*, 490–494. [[CrossRef](#)]
19. Klein, Y.M.; Sciortino, N.F.; Housecroft, C.E.; Kepert, C.J.; Neville, S.M. Structure and Magnetic Properties of the Spin Crossover Linear Trinuclear Complex [Fe₃(furtrz)₆(ptol)₂(MeOH)₄]·4(ptol)·4(MeOH) (furtrz: furanylidene-4H-1,2,4-triazol-4-amine ptol: p-tolylsulfonate). *Magnetochemistry* **2016**, *2*, 7. [[CrossRef](#)]
20. Wang, J.L.; Liu, Q.; Meng, Y.S.; Zheng, H.; Zhu, H.L.; Shi, Q.; Liu, T. Synergic on/off Photoswitching Spin State and Magnetic Coupling between Spin Crossover Centers. *Inorg. Chem.* **2017**, *56*, 10674–10680. [[CrossRef](#)] [[PubMed](#)]
21. Chen, W.B.; Leng, J.D.; Wang, Z.Z.; Chen, Y.C.; Miao, Y.; Tong, M.L.; Dong, W. Reversible crystal-to-crystal transformation from a trinuclear cluster to a 1D chain and the corresponding spin crossover (SCO) behaviour change. *Chem. Commun.* **2017**, *53*, 7820–7823. [[CrossRef](#)] [[PubMed](#)]

22. Chen, W.B.; Chen, Y.C.; Yang, M.; Tong, M.L.; Dong, W. Water molecule induced reversible single-crystal-to-single-crystal transformation between two trinuclear Fe (ii) complexes with different spin crossover behavior. *Dalton Trans.* **2018**, *47*, 4307–4314. [[CrossRef](#)] [[PubMed](#)]
23. Pittala, N.; Thétiot, F.; Charles, C.; Triki, S.; Boukheddaden, K.; Chastanet, G.; Marchivie, M. An unprecedented trinuclear Fe II triazole-based complex exhibiting a concerted and complete sharp spin transition above room temperature. *Chem. Commun.* **2017**, *53*, 8356–8359. [[CrossRef](#)] [[PubMed](#)]
24. Thomann, M.; Kahn, O.; Guilhem, J.; Varret, F. Spin conversion versus antiferromagnetic interaction in iron (II) trinuclear species. crystal structures and magnetic properties of $[\text{Fe}_3(p\text{-MeOptrz})_8(\text{H}_2\text{O})_4](\text{BF}_4)_6$ and $[\text{Fe}_3(p\text{-MeOptrz})_6(\text{H}_2\text{O})_6](\text{tos})_6$ [$p\text{-MeOptrz}$ = 4-(p-Methoxyphenyl)-1, 2, 4-triazole, tos = tosylate]. *Inorg. Chem.* **1994**, *33*, 6029–6037.
25. Kolnaar, J.J.A.; van Dijk, G.; Koojiman, H.; Spek, A.L.; Ksenofontov, V.; Gütllich, P.; Haasnoot, J.G.; Reedijk, J. Synthesis, Structure, Magnetic Behavior, and Mössbauer Spectroscopy of Two New Iron (II) Spin-Transition Compounds with the Ligand 4-Isopropyl-1, 2, 4-triazole. X-ray Structure of $[\text{Fe}_3(4\text{-isopropyl-1, 2, 4-triazole})_6(\text{H}_2\text{O})_6](\text{tosylate})_6 \cdot 2\text{H}_2\text{O}$. *Inorg. Chem.* **1997**, *36*, 2433–2440. [[CrossRef](#)] [[PubMed](#)]
26. Savard, D.; Cook, C.; Enright, G.D.; Korobkov, I.; Burchell, T.J.; Murugesu, M. Gradual spin crossover behaviour in a linear trinuclear Fe II complex. *Cryst. Eng. Comm.* **2011**, *13*, 5190–5197. [[CrossRef](#)]
27. Bain, G.A.; Berry, J.F. Diamagnetic corrections and Pascal's constants. *J. Chem. Educ.* **2008**, *85*, 532. [[CrossRef](#)]
28. Gunnlaugsson, H.P. Spreadsheet based analysis of Mössbauer spectra. *Hyperfine Interact.* **2016**, *237*, 79. [[CrossRef](#)]
29. SMART 5.0 and SAINT 4.0 for Windows NT, Area Detector Control and Integration Software; Bruker Analytical X-Ray Systems Inc.: Madison, WI, USA, 1998.
30. Sheldrick, G.M. SADABS: Program for Empirical Absorption Correction of Area Detector Data; University of Göttingen: Göttingen, Germany, 1996.
31. Sheldrick, G.M. Crystal structure refinement with SHELXL. *Acta Crystallogr.* **2015**, *C71*, 3–8.
32. Sheldrick, G.M. SHELXTL 5.1 for Windows NT: Structure Determination Software Programs; Bruker Analytical X-ray Systems, Inc.: Madison, WI, USA, 1997.
33. Dolomanov, O.V.; Bourhis, L.J.; Gildea, R.J.; Howard, J.A.K.; Puschmann, H.J. OLEX2: A complete structure solution, refinement and analysis program. *Appl. Crystallogr.* **2009**, *42*, 339–341. [[CrossRef](#)]
34. Diamond—Crystal and Molecular Structure Visualization. Available online: <http://www.crystalimpact.com/diamond> (accessed on 5 August 2018).
35. Khan, T.; Yadav, R. Synthesis, characterization and antioxidant activity of some new 4-thiazolidinonyl-4H-1, 2, 4-triazole derivatives. *Heterocycl. Lett.* **2016**, *6*, 757–766.
36. Kwiecień, A.; Barys, M.; Ciunik, Z. Stable Hemiaminals with a Cyano Group and a Triazole Ring. *Molecules* **2014**, *19*, 11160–11177. [[CrossRef](#)] [[PubMed](#)]
37. Chakraborty, P.; Tissot, A.; Peterhans, L.; Guenee, L.; Besnard, C.; Pattison, P.; Hauser, A. Determination of the molecular structure of the short-lived light-induced high-spin state in the spin-crossover compound $[\text{Fe}(6\text{-mepy})_3\text{tren}](\text{PF}_6)_2$. *Phys. Rev. B* **2013**, *87*, 214306. [[CrossRef](#)]
38. Gómez, V.; de Pipaón, C.S.; Maldonado-Illescas, P.; Waerenborgh, J.C.; Martin, E.; Benet-Buchholz, J.; Galan-Mascarós, J.R. Easy Excited-State Trapping and Record High T TIESST in a Spin-Crossover Polyanionic Fe^{II} Trimer. *J. Am. Chem. Soc.* **2015**, *137*, 11924–11927. [[CrossRef](#)] [[PubMed](#)]
39. Borello, E.; Zecchina, A. Infrared spectra of v-triazoles—I: 2-Aryl-v-triazoles. *Spectrochim. Acta* **1963**, *19*, 1703–1715. [[CrossRef](#)]
40. Prashanthi, Y.; Raj, S. Synthesis and characterization of transition metal complexes with N, O; N, N and S, N-donor Schiff base ligands. *J. Sci. Res.* **2010**, *2*, 114–126.
41. Sumrra, S.H.; Chohan, Z.H. Spectrochimica acta A: Molecular and biomolecular spectroscopy. *Spectrochim. Acta* **2012**, *98*, 53–61.
42. Salaudeen, A.A.; Kilner, C.A.; Halcrow, M.A. Mononuclear and dinuclear iron thiocyanate and selenocyanate complexes of tris-pyrazolylmethane ligands. *Polyhedron* **2008**, *12*, 2569–2576. [[CrossRef](#)]
43. Nakamoto, K. *Infrared and Raman Spectra of Inorganic and Coordination Compounds Part B*, 5th ed.; Wiley Interscience: New York, NY, USA, 1997; p. 116.
44. Arduini, A.L.; Garnett, M.; Thompson, R.C.; Wong, T.C.T. Magnetic and Spectral Studies on Cobalt (II) and Copper (II) Salts of Methylsulfuric, Trifluoromethylsulfuric, and Paratolylsulfuric Acids. *Can. J. Chem.* **1975**, *53*, 3812–3819. [[CrossRef](#)]

45. Chilton, N.F.; Anderson, R.P.; Turner, L.D.; Soncini, A.; Murray, K.S. PHI: A powerful new program for the analysis of anisotropic monomeric and exchange-coupled polynuclear d- and f-block complexes. *J. Comput. Chem.* **2013**, *34*, 1164–1175. [[CrossRef](#)] [[PubMed](#)]
46. Schünemann, V.; Winkler, H. Structure and dynamics of biomolecules studied by Mössbauer spectroscopy. *Rep. Prog. Phys.* **2000**, *63*, 263–353. [[CrossRef](#)]
47. Jung, J.; Spiering, H.; Yu, Z.; Gülich, P. The debye-waller factor in spin crossover molecular crystals: A mössbauer study on $[\text{Fe}_x\text{Zn}_{1-x}(\text{ptz})_6](\text{BF}_4)_2$. *Hyperfine Interact.* **1995**, *95*, 107–128. [[CrossRef](#)]
48. Kolnaar, A.; Jeroen, J.; de Heer, M.I.; Kooijman, H.; Spek, A.L.; Schmitt, G.; Ksenofontov, V.; Gülich, P.; Haasnoot, J.G.; Reedijk, J. Synthesis, Structure and Properties of a Mixed Mononuclear/Dinuclear Iron (II) Spin-Crossover Compound with the Ligand 4-(p-Tolyl)-1, 2,4-triazole. *Eur. J. Inorg. Chem.* **1999**, *5*, 881–886. [[CrossRef](#)]



© 2018 by the authors. Licensee MDPI, Basel, Switzerland. This article is an open access article distributed under the terms and conditions of the Creative Commons Attribution (CC BY) license (<http://creativecommons.org/licenses/by/4.0/>).